

# Lifetime Difference and Endpoint effect in the Inclusive Bottom Hadron Decays

Y.B Zuo, Y.A Yan, Y.L Wu and W.Y Wang

Institute of Theoretical Physics, Chinese Academy of Sciences,  
P.O.Box 2735, Beijing 100080, P.R.China

July 2, 2018

## Abstract

The lifetime differences of bottom hadrons are known to be properly explained within the framework of heavy quark effective field theory(HQEFT) of QCD via the inverse expansion of the dressed heavy quark mass. In general, the spectrum around the endpoint region is not well behaved due to the invalidity of  $1/m_Q$  expansion near the endpoint. The curve fitting method is adopted to treat the endpoint behavior. It turns out that the endpoint effects are truly small and the explanation on the lifetime differences in the HQEFT of QCD is then well justified. The inclusion of the endpoint effects makes the prediction on the lifetime differences and the extraction on the CKM matrix element  $|V_{cb}|$  more reliable.

## 1 Introduction

The heavy quark effective field theory (HQEFT) of QCD[1, 2] enable us to include in the heavy hadron decays the nonperturbative binding effects for light degrees of freedom via introducing the concept of dressed heavy quark. As a consequence, it has provided a consistent explanation for the lifetime differences in heavy bottom hadron decays and led to a reliable extraction on the CKM matrix elements  $|V_{cb}|$  and  $|V_{ub}|$  [3, 4]. Nevertheless the spectrum around the endpoint region is not well behaved due to the invalidity of  $1/m_Q$  expansion near the endpoint. Especially, an abnormal behavior that the decay width becomes negative appears in the endpoint region of the lepton spectrum. References [5, 6] give the description of this region using the parton model and its comparison with experiments. In the previous paper[3, 4] the endpoint effects on the lifetime differences are considered to be small. To justify this consideration, we adopt a curve fitting method to investigate in detail the endpoint effects. The paper is organized as follows: in section 2, we present for completeness an explicit evaluation of the differential decay width. We then compare in section 3 the lepton spectrum obtained by means of dressed heavy quark expansion to

the next leading order with the one by the free quark model. To be more clear, we also present the lepton spectrum keeping only the leading order contribution in the heavy quark expansion of HQEFT. It is shown that in the endpoint region the contribution from the next leading order is so large that the expansion doesn't converge and the expansion method become invalid. To describe the corresponding physics at endpoint, a curve fitting method is introduced to treat the endpoint behavior based on the analyticity and continuity of physics spectrum. Two schemes in the curve fitting method are considered in order to see how the endpoint effects influence the observable quantities. Our conclusions are presented in the last section.

## 2 The formulation of lepton spectrum in inclusive semileptonic decays

Following the evaluation presented in refs.[3, 4, 7], the inclusive decays of heavy hadrons within the framework of HQEFT of QCD is described as follows. The semileptonic decays

$$H(P_H = m_H v) \rightarrow X_c(P_X) + \ell(p) + \bar{\nu}_\ell(p') \quad (1)$$

can be described by the effective Hamiltonian

$$\mathcal{H}_{eff} = \frac{4G_f}{\sqrt{2}} V_{cb} \bar{c} \Gamma^\mu b \bar{\ell} \Gamma_\mu \nu_\ell \quad (2)$$

To calculate its decay width, we introduce a hadron tensor

$$W^{\mu\nu} = \frac{1}{2m_H} (2\pi)^3 \sum_{X_c} \delta^4(P_{Hb} - q - P_X) \langle H | J^{\mu\dagger} | X_c \rangle \langle X_c | J^\nu | H \rangle \quad (3)$$

where  $q = p + p'$ ,  $J^\mu = \bar{c} \Gamma^\mu b$ . Summing all the contributions with respect to the spin of hadrons in the initial state and averaging in the final state, according to the Lorentz invariance, the hadron tensor can be described by five shape factors:

$$W^{\mu\nu} = -g^{\mu\nu} W_1 + v^\mu v^\nu W_2 - i \epsilon^{\mu\nu\alpha\beta} v_\alpha q_\beta W_3 + q^\mu q^\nu W_4 + (q^\mu v^\nu + q^\nu v^\mu) W_5 \quad (4)$$

Then, the differential decay width turns out to be

$$\begin{aligned} \frac{d\Gamma}{dq^2 dE_\ell dE_\nu} &= \frac{G_F^2 |V_{cb}|^2}{2\pi^3} \left\{ [q^2 - m_\ell^2] W_1 + \frac{1}{2} [4E_\ell E_\nu - q^2 + m_\ell^2] W_2 \right. \\ &\quad \left. + [q^2 (E_\ell - E_\nu) - m_\ell^2 (E_\ell + E_\nu)] W_3 + m_\ell^2 \frac{2E_\nu}{\hat{m}_b} W_5 \right\} \quad (5) \end{aligned}$$

Furthermore, the shape factors  $W_i$  can be evaluated by studying the following time-ordered product

$$\begin{aligned} T^{\mu\nu} &= -\frac{i}{2m_H} \int d^4x e^{-iq \cdot x} \langle H | \mathcal{T} \{ J^{\mu\dagger}(x) J^\nu(0) \} | H \rangle \\ &= -g^{\mu\nu} T_1 + v^\mu v^\nu T_2 - i \epsilon^{\mu\nu\alpha\beta} v_\alpha q_\beta T_3 + q^\mu q^\nu T_4 + (v^\mu q^\nu + v^\nu q^\mu) T_5 \quad (6) \end{aligned}$$

as the factors  $W_i$  are related to  $T_i$  via

$$W_i = -\frac{1}{\pi} I_m T_i \quad (7)$$

The quark matrix elements in (6) can be represented in the momentum space as follows

$$\bar{u} \frac{\gamma^\mu (m_b \not{p} + \not{k} - \not{q}) \gamma^\nu}{(m_b v + k - q)^2 - m_c^2 + i\epsilon} \frac{1 - \gamma_5}{2} u \quad (8)$$

and the one gluon matrix elements are given by

$$\bar{u} \frac{g}{2} G^{\alpha\beta} \epsilon_{\alpha\beta\kappa\sigma} (m_b v + k - q)^\kappa \frac{g^{\mu\sigma} \gamma^\nu + g^{\nu\sigma} \gamma^\mu - g^{\mu\nu} \gamma^\sigma + i\epsilon^{\mu\nu\sigma\tau} \gamma_\tau}{[(m_b v + k - q)^2 - m_c^2 + i\epsilon]^2} \frac{1 - \gamma_5}{2} u \quad (9)$$

From refs. [3], we have

$$T_1 = \frac{1}{2} (\hat{m}_b - E_\ell - E_\nu) \frac{1}{\Delta} - \frac{1}{2} (3A + N_b) (\hat{m}_b - E_\ell - E_\nu) \frac{1}{\Delta^2} + 2A (\hat{m}_b - E_\ell - E_\nu) [q^2 - (E_\ell + E_\nu)^2] \frac{1}{\Delta^3} \quad (10)$$

with  $\Delta = (\hat{m}_b v - q)^2 - m_c^2 + i\epsilon$ ,  $\hat{m}_b \equiv m_b + v \cdot k$ ,  $A = \frac{\kappa_1}{3}$ ,  $N_b = \frac{d_H \kappa_2}{3}$ . Similarly,  $T_2, T_3, T_5$  can all be expanded with respect to  $1/\Delta$ .

The lepton spectrum of inclusive semileptonic decay is given by[3]

$$\begin{aligned} \frac{1}{\hat{\Gamma}_0} \frac{d\Gamma}{dy} = & -2\rho^2(3 - \rho) + \frac{4\rho^3}{(1 - y)^3} - \frac{6\rho^2(1 + \rho)}{(1 - y)^2} + \frac{12\rho^2}{1 - y} + 6(1 - \rho)y^2 - 4y^3 \\ & + \frac{A}{\hat{m}_b^2} \{-6\rho^3 + 12\rho^2 - \frac{24\rho^3}{(1 - y)^5} + \frac{6\rho^2(3 + 5\rho)}{(1 - y)^4} - \frac{12\rho^2}{(1 - y)^3} - \frac{18\rho^2}{(1 - y)^2} + 6y^2\} \\ & + \frac{N_b}{\hat{m}_b^2} \{-6\rho(2 + \rho) - \frac{12\rho^2}{(1 - y)^3} + \frac{6\rho(2 + 3\rho)}{(1 - y)^2} - 24\rho y - 18y^2\} \quad (11) \end{aligned}$$

with

$$\hat{\Gamma}_0 \equiv \frac{G_F^2 \hat{m}_b^5 |V_{cb}|^2}{192\pi^3}, \quad y \equiv \frac{2E_\ell}{\hat{m}_b}, \quad \rho \equiv \frac{m_c^2}{\hat{m}_b^2}$$

When taking the lepton energy  $E_\ell$  to be in the physics region, the corresponding region for  $y$  is given by

$$0 \leq y \leq \frac{m_{H_b}}{\hat{m}_b} [1 - (\frac{m_{H_c}}{m_{H_b}})^2] \quad (12)$$

for light leptons with their masses  $m_\ell$  being ignored. For lepton  $\tau$ , its mass can not be ignored and the corresponding region is given by

$$2\sqrt{r_\tau} \leq y \leq \frac{m_{H_b}}{\hat{m}_b} [1 + (\frac{m_\tau}{m_{H_b}})^2 - (\frac{m_{H_c}}{m_{H_b}})^2] \quad (13)$$

with  $r_\tau = \frac{m_\tau^2}{\hat{m}_b^2}$ . Here  $m_{H_b}$  and  $m_{H_c}$  are the corresponding masses of hadrons containing  $b$  quark and  $c$  quark respectively.

### 3 Endpoint effects and Lifetime difference

#### 3.1 Definitions and notations

The total decay width of bottom hadron  $H_b$  is

$$\Gamma_{H_b}^t = \frac{1}{\tau(H_b)} \simeq \Gamma(H_b \rightarrow X_c) + \Gamma(H_b \rightarrow X_{c\bar{c}}) + \sum_{\ell} \Gamma(H_b \rightarrow X_c \ell \bar{\nu}) \quad (14)$$

To be more precise, the QCD corrections to the decay width should be considered. The general formulae of the decay width with QCD corrections can be expressed as follows

$$\begin{aligned} \frac{1}{\hat{\Gamma}_0} \Gamma(H_b \rightarrow X_c \ell \bar{\nu}) &= \eta_{c\ell}(\mu) \Gamma(\rho) \\ \frac{1}{\hat{\Gamma}_0} \Gamma(H_b \rightarrow X_c \tau \bar{\nu}) &= \eta_{c\tau}(\mu) \Gamma(\rho, \rho_\tau) \\ \frac{1}{\hat{\Gamma}_0} \Gamma(H_b \rightarrow X_c X_{ud}) &= 3\eta_{cu}(\mu) \Gamma(\rho) - \frac{1}{\hat{m}_b^2} (c_+^2(\mu) - c_-^2(\mu)) 6(1-\rho)^3 \kappa_2 \\ \frac{1}{\hat{\Gamma}_0} \Gamma(H_b \rightarrow X_c X_{\bar{c}s}) &= 3\eta_{cc}(\mu) \Gamma(\rho, \hat{\rho}) - \frac{1}{\hat{m}_b^2} (c_+^2(\mu) - c_-^2(\mu)) I_3(\rho) 6\kappa_2 \end{aligned} \quad (15)$$

with

$$\rho_\tau \equiv \frac{m_\tau^2}{\hat{m}_b^2}, \quad \hat{\rho} \equiv \frac{\hat{m}_c^2}{\hat{m}_b^2}$$

and

$$c_\pm(\mu) = \left( \frac{\alpha_s(m_W)}{\alpha_s(\mu)} \right)^{a_\pm}, \quad a_- = -2a_+ = -\frac{12}{33-2n_f}$$

$$I_3(x) = \sqrt{1-4x} \left( 1 + \frac{x}{2} + 3x^2 \right) - 3x(1-2x^2) \ln \frac{1 + \sqrt{1-4x}}{1 - \sqrt{1-4x}}$$

Using the two loop results obtained in [8, 9] for the QCD corrections and taking the input value  $m_c/m_b = 0.3$ , the QCD correction factors  $\eta_{c\ell}, \eta_{c\tau}, \eta_{cu}, \eta_{cc}$  are given by

$$\begin{aligned} \eta_{c\ell} &= 1 - 1.67 \left[ \frac{\alpha_s(\mu)}{\pi} \right] - 15.1 \left[ \frac{\alpha_s(\mu)}{\pi} \right]^2 \\ \eta_{c\tau} &= 1 - 1.39 \left[ \frac{\alpha_s(\mu)}{\pi} \right] - 1.58 \left[ \frac{\alpha_s(\mu)}{\pi} \right]^2 \beta_0 \quad (16) \\ \eta_{cc} &= 1 + 2.99 \left[ \frac{\alpha_s(\mu)}{\pi} \right] + \left\{ 3.67\beta_0 + 3.34 \ln \left( \frac{m_W}{m_b} \right) + 4 \left[ \ln \left( \frac{m_W}{m_b} \right) \right]^2 \right\} \left[ \frac{\alpha_s(\mu)}{\pi} \right]^2 \\ \eta_{cu} &= 1 - 0.67 \left[ \frac{\alpha_s(\mu)}{\pi} \right] + \left\{ -1.11\beta_0 + 7.17 \ln \left( \frac{m_W}{m_b} \right) + 4 \left[ \ln \left( \frac{m_W}{m_b} \right) \right]^2 \right\} \left[ \frac{\alpha_s(\mu)}{\pi} \right]^2 \end{aligned}$$

With the above analysis, we are able to calculate the branching ratio of semileptonic decay

$$B_{SL}(H) \equiv B_r(H_b \rightarrow X_c e \bar{\nu}) = \frac{\Gamma(H_b \rightarrow X_c e \bar{\nu})}{\Gamma_H^t},$$

$$B_\tau(H) \equiv B_r(H_b \rightarrow X_c \tau \bar{\nu}) = \frac{\Gamma(H_b \rightarrow X_c \tau \bar{\nu})}{\Gamma_H^t}$$

the charm counting

$$n_c(H) \equiv 1 + \frac{\Gamma(H_b \rightarrow X_{c\bar{c}})}{\Gamma_H^t} - \frac{\Gamma_{nocharm}}{\Gamma_H^t} \simeq 1 + \frac{\Gamma(H_b \rightarrow X_{c\bar{c}})}{\Gamma_H^t}$$

and the ratio between the  $\tau$  and  $\beta$  decay :

$$R(H) \equiv \frac{B_\tau(H)}{B_{SL}(H)}$$

Note that the dressed heavy quark mass  $\hat{m}_Q$  is related to the hadron mass via

$$\hat{m}_Q = m_H \left[ 1 + \frac{\kappa_1 - d_H \kappa_2}{m_H^2} + O\left(\frac{1}{m_H^3}\right) \right] \quad (17)$$

They differ starting from the order of  $1/m_H^2$ .

### 3.2 The endpoint behavior of the lepton spectrum in heavy quark expansion

It is known that the heavy quark expansion becomes unreliable in the endpoint region. To see it explicitly, we plot in Fig. 1 the lepton spectrum of B meson decay via heavy quark expansion in HQEFT of QCD. For comparison, we also plot the corresponding spectrum in free quark model. Here we have ignored the lepton mass. The other relevant parameters are taken to be:  $m_c = 1.65 \text{ GeV}$ ,  $\kappa_1 = -0.55 \text{ GeV}^2$  and  $m_b = 4.7 \text{ GeV}$  (for the free quark model). In general, the numerical calculations involve, besides the heavy meson and baryon masses, four theoretical parameters. They are the pole mass  $m_c$  of charm quark, the energy scale  $\mu$ , and the two hadronic parameters  $\kappa_1$  and  $\kappa_2$ . Their values are taken to be the same as the ones used in [3, 4] in our numerical calculations of this paper.

$$m_{B^0} = 5.2792 \text{ GeV} ; m_{D^+} = 1.8693 \text{ GeV}$$

$$m_{\Lambda_c} = 2.2849 \text{ GeV} ; m_{\Lambda_b} = 5.624 \text{ GeV} ; m_\tau = 1.777 \text{ GeV} \quad (18)$$

$$0.3 \text{ GeV}^2 \leq -\kappa_1 \leq 0.7 \text{ GeV}^2 \quad (19)$$

$$\kappa_2 = \frac{1}{8}(m_{B^{*0}}^2 - m_{B^0}^2) = 0.06 \text{ GeV}^2 \quad (20)$$

$$1.55 \text{ GeV} \leq m_c \leq 1.75 \text{ GeV} \quad (21)$$

From Fig.1, it is easily seen that the decay width in free quark model (dash-dotted line) is smaller than the one obtained by using the heavy quark expansion. The reason is simple that in the former case the nonperturbative binding effects of quarks within the hadron have been ignored. In the latter case, we have plotted two curves which correspond to two cases: the leading order approximation (dashed line) and the next-to-leading order approximation (solid line). It is seen that when including the next-to-leading order contributions in the heavy quark expansion, the decay width becomes negative in the endpoint region of the lepton spectrum. This is because the lepton energy becomes too large so that the heavy quark expansion can not be used in this region. To be more clear, we plot in Fig.2 the corrections of the next-to-leading order relative to the leading order. On the other hand, the zero value of the differential decay width is not at the physics endpoint. This happens also in the free quark model. It implies that the simple quark-hadron duality is not complete.

For  $\Lambda_b$  baryon decays, the situation is different, there is no abnormal behavior near the endpoint of the lepton spectrum. This can be seen explicitly in Fig.3. But it shows that near the endpoint the next-to-leading order corrections become larger than the leading order contributions. For the same reason, the differential decay width does not reach zero at the physics endpoint.

It is then clear that we need to smooth the endpoint behavior and make the spectrum come to zero at the physics endpoint.

### 3.3 Curve fitting method and Improvement of endpoint behavior

As analyzed above, the heavy quark expansion becomes invalid in the endpoint region of lepton spectrum as the expansion does not converge in this region. In the bottom hadron decays, the abnormal behavior occurs near the endpoint. To be specific, we define the endpoint region as the region ranges from the point  $y_n$  where the next leading order corrections are one third of the leading order to the physics endpoint  $y_e$ . In the endpoint region, there is no satisfactory approach to treat its behavior in a reasonable way. In the present paper, we shall adopt a curve fitting method to treat the endpoint behavior.

To see how the endpoint effects rely on the fitting schemes, we consider two cases. Firstly, we may consider a simple treatment as the fitting scheme 1. In this fitting scheme, to avoid the abnormal behavior in the B meson decays, at the point  $y_n$ , we simply replace the next-to-leading spectrum by the leading order spectrum with multiplying a rescaling factor. Here the rescaling factor is determined by the continuity condition at the connection point of the two regions. It is plotted in the figure 4,5. For  $\Lambda_b$  decays, as there is no abnormal behavior, we simply keep the initial spectrum.

To ensure all the differential decay widths vanishing at the physics endpoint, we then introduce a smooth fitting function

$$F_e(y) = \int_0^{y_e-y} f(x)dx, \quad f(x) = e^{a-0.1[\frac{1}{x} + \frac{b}{(1-x)^2}]} \quad (22)$$

where  $a, b$  are two parameters. Choosing appropriate values for them, we can make the function to be zero at the physics endpoint and to be equal to unit in the region where the heavy quark expansion is reasonable so that the lepton spectrums multiplied by these functions do not change except in the endpoint region.

To be specific, we let the fitting function begin to slightly reduce at the point where the next leading order corrections are 30% of the leading order. For different decays modes, it needs to adjust the two parameters to satisfy corresponding conditions. The typical values corresponding to  $m_c = 1.65\text{GeV}$ ,  $\kappa_1 = -0.55\text{GeV}^2$  are listed explicitly here.

For  $B^0$  decays:

$$m_\ell = 0 : a = 25.40; b = 185.7 \quad (23)$$

$$m_\ell = m_\tau : a = 34.96; b = 270.8 \quad (24)$$

$$m_\ell = \hat{m}_c : a = 33.56; b = 258.2 \quad (25)$$

For  $\Lambda_b$  decays:

$$m_\ell = 0 : a = 140.70; b = 1263 \quad (26)$$

$$m_\ell = m_\tau : a = 299.47; b = 2796 \quad (27)$$

$$m_\ell = \hat{m}_c : a = 416.12; b = 3932 \quad (28)$$

The behavior of the fitting function for the lepton spectrum in Fig.5 is plotted in Fig.6. Once multiplying the lepton spectrum by the corresponding fitting function, the behavior of the spectrum in the endpoint region is well improved and its value at the physics endpoint is ensured to be zero. This can be seen explicitly from Fig. 7.

We now consider another fitting scheme, i.e., scheme 2. Here we adopt the same criterion for  $B$  meson and  $\Lambda_b$  baryon. Let  $y_m$  denote the point where the spectrum becomes maximum. We divided the spectrum into three regions  $R_m = (0, y_m)$ ,  $R_n = (y_m, y_n)$  and  $R_e = (y_n, y_e)$ . We now treat the three regions separately. In the first region  $R_m$  the spectrum is well behaved as the heavy quark expansion is thought to be reliable.

In the second region  $R_n$ , we may introduce a fitting function  $F_n(y)$

$$F_n(y) = \alpha + \beta(y - \gamma)^2 \quad (29)$$

with  $y \geq \gamma$  and  $\beta < 0$ . The three parameters  $\alpha, \beta$  and  $\gamma$  are determined by the following conditions:

$$F_n(y_m) = \frac{1}{\hat{\Gamma}_0} \frac{d\Gamma}{dy}(y_m) \Big|_{A=\frac{\kappa_1}{3}, N_b=\frac{d_H \kappa_2}{3}} \quad (30)$$

and

$$F_n(y_n) = \frac{\frac{1}{\hat{\Gamma}_0} \frac{d\Gamma}{dy}(y_n) \Big|_{A=0, N_b=0}}{1 - \frac{\frac{1}{\hat{\Gamma}_0} \frac{d\Gamma}{dy}(y_n) \Big|_{A=\frac{\kappa_1}{3}, N_b=\frac{d_H \kappa_2}{3}} - \frac{1}{\hat{\Gamma}_0} \frac{d\Gamma}{dy}(y_n) \Big|_{A=0, N_b=0}}{\frac{1}{\hat{\Gamma}_0} \frac{d\Gamma}{dy}(y_n) \Big|_{A=0, N_b=0}}}$$

$$= \frac{3}{4} \frac{1}{\hat{\Gamma}_0} \frac{d\Gamma}{dy}(y_n)|_{A=0, N_b=0} \quad (31)$$

The typical values for  $\alpha$ ,  $\beta$ ,  $\gamma$  corresponding to  $m_c = 1.65\text{Gev}$ ,  $\kappa_1 = -0.55\text{Gev}^2$  are listed explicitly here.

For  $B^0$  decays:

$$m_\ell = 0 : \alpha = 0.9724, \beta = -18.34, \gamma = 0.6557 \quad (32)$$

$$m_\ell = m_\tau : \alpha = 0.4982, \beta = -20.04, \gamma = 0.8367 \quad (33)$$

$$m_\ell = \hat{m}_c : \alpha = 0.5449, \beta = -19.76, \gamma = 0.8156 \quad (34)$$

For  $\Lambda_b$  decays:

$$m_\ell = 0 : \alpha = 1.046, \beta = -20.75, \gamma = 0.6770 \quad (35)$$

$$m_\ell = m_\tau : \alpha = 0.6025, \beta = -21.98, \gamma = 0.8322 \quad (36)$$

$$m_\ell = \hat{m}_c : \alpha = 0.4858, \beta = -22.63, \gamma = 0.8829 \quad (37)$$

In the third region  $R_e$ , namely the endpoint region, we adopt the leading order spectrum with a rescaling factor to ensure the continuity at the connection point  $y_n$ . This is shown in Fig.8. Then multiplying the smooth fitting function  $F_e(y)$  defined in scheme 1. For illustration, we have plotted in the figures 9,10 the spectra of semileptonic decays of B meson and  $\Lambda_b$  baryon.

Note that in all the figures we have only illustrated the semileptonic decays with neglecting the lepton masses. Its generalization to all the processes is straightforward.

It is seen that in the scheme 2 the spectrum is well improved in the endpoint region. In addition, the curve fitting method in the scheme 2 adopt the same criterion for the  $\Lambda_b$  decays as well, so it is expected to be more reliable than the scheme 1. We shall present a numerical calculation in next section to see quantitatively the endpoint effects.

### 3.4 Numerical results and endpoint effects

Now we calculate the observable quantities using the lepton spectrum obtained above. First of all we should integrate the lepton spectrum in the whole physical region to calculate  $\Gamma$  for all decay channels. Then the radiative corrections are added according to (15). In the end, predictions for the observable quantities are obtained according to their definitions. The results are shown in Table 1, 2, 3, 4, 5, 6, 7, 8<sup>1</sup>. The choice of  $\mu$  is subjective and we have adjusted it according to experiments.

In the following, we analyze our results by comparing them with experiments. The experimental values of the observable quantities[3, 10, 11] are :

$$\frac{\tau(\Lambda_b)}{\tau(B^0)} = 0.79 \pm 0.05 \quad (38)$$

---

<sup>1</sup>In the present paper, we use  $\tau(B^0) = 1.540\text{ps}$  and  $B_{SL}(B^0) = 10.48\%$  in extracting the CKM matrix element  $|V_{cb}|$ .

$$B_{SL}(B^0) = 10.48 \pm 0.5\% \quad (39)$$

$$B_{SL}(\Lambda_b) = 9.0_{-2.8}^{+3.0}\% \quad (40)$$

$$n_c(B^0) = 1.17 \pm 0.04 \quad (41)$$

$$B_\tau(B^0) = 2.6 \pm 0.1\% \quad (42)$$

$$|V_{cb}| = (41.2 \pm 2.0) \times 10^{-3} \quad (43)$$

First, let us see the results in scheme 1 given in Table 1, 2, 3, 4. Table 1, 2 is corresponding to  $\mu = \frac{1}{2}m_b$  and  $\mu = m_b$  respectively.<sup>2</sup> The lifetime difference  $\frac{\tau(\Lambda_b)}{\tau(B^0)}$  in these two tables all fall in the range of the experimental uncertainties and are slightly dependent on parameters  $m_c, \kappa_1$  and  $\mu$ . The semileptonic branching ratio  $B_{SL}(B^0)$  is sensitive to the choice of  $\mu$ . Low values of  $\mu$  are corresponding to small values of  $B_{SL}(B^0)$ . The charm counting  $n_c(B^0)$  is compatible with the experimental data. The numerical values depend on the pole mass of charm quark and the parameter of  $\kappa_1$ . For small pole mass of charm quark, the values of the charm counting  $n_c(B^0)$  become slightly large. In Table 3 we considered the case with fixing the semileptonic branching ratio to be the experimental central value  $B_{SL}(B^0) = 10.48\%$  by varying the parameter  $\mu$ . It is seen that for various values of parameters the energy scale  $\mu$  is found to be  $\mu = 2.72 \pm 0.34 \text{ GeV}$  when the semileptonic branching ratio  $B_{SL}(B^0)$  is fixed to 10.48%. Taking  $\mu = 2.70 \text{ GeV}$ ,  $m_c = 1.65 \text{ GeV}$  and  $\kappa_1 = -0.55 \text{ GeV}^2$  as the typical values, we present in Table 4 the corresponding predictions for the various observable quantities. Apparently, the predictions for the semileptonic branching ratio have been improved remarkably. In addition, the lifetime difference  $\frac{\tau(\Lambda_b)}{\tau(B^0)}$  is much better than Table 1, 2.

The results of scheme 2 are presented in Table 5, 6, 7, 8. Where Table 5 and 6 are corresponding to  $\mu = \frac{1}{2}m_b$  and  $\mu = m_b$  respectively. The predictions for  $\frac{\tau(\Lambda_b)}{\tau(B^0)}$  are slightly larger than scheme 1 as a whole. When choosing  $\mu = 2.72 \text{ GeV}$ ,  $m_c = 1.65 \text{ GeV}$  and  $\kappa_1 = -0.55 \text{ GeV}^2$  as the typical values via  $B_{SL}(B^0)$  being fixed to be  $B_{SL}(B^0) = 10.48\%$ , the corresponding predictions for various observable quantities are given in Table 8.

Comparing the two schemes, the predictions in the scheme 2 are not too much different from the scheme 1. It implies that the results are not sensitive to the fitting scheme. This can also be seen from Figs.9 and 10, where the two spectra are very similar with each other. As the fitting method of scheme 2 has adopted the same criterion for both  $B$  and  $\Lambda_b$  decays, the results in this scheme are expected to be more reliable. So we may take the results in scheme 2 as our theoretical predictions. They are given by

$$\frac{\tau(\Lambda_b)}{\tau(B^0)} = 0.80 \pm 0.03 \quad (44)$$

$$B_{SL}(B^0) = 10.52 \pm 0.45\% \quad (45)$$

$$B_{SL}(\Lambda_b) = 11.23 \pm 0.32\% \quad (46)$$

---

<sup>2</sup>Here,  $m_b = 4.4 \text{ GeV}$ , which is different from the value in free quark model.

$$n_c(B^0) = 1.20 \pm 0.02 \quad (47)$$

$$B_\tau(B^0) = 2.6 \pm 0.2\% \quad (48)$$

$$|V_{cb}| = (40.6 \pm 2.2) \times 10^{-3} \quad (49)$$

## 4 Conclusion

In the present paper, we adopt a curve fitting method to improve the abnormal behavior near the endpoint region and to make a more reliable calculation for the observable quantities. The resulting prediction for the lifetime difference is  $\tau(\Lambda_b)/\tau(B^0) = 0.80 \pm 0.03$  which is consistent with the experimental value  $0.79 \pm 0.05$ . It is of interest to note that the endpoint effects to the lifetime difference is small in the framework of HQEFT of QCD. The predicted value for the lifetime difference is not sensitive to other theoretical parameters such as the pole mass of charm quark, the parameter  $\kappa_2$  and the running scale  $\mu$ . For other predictions, the large uncertainties mainly arise from the running scale  $\mu$ . The resulting central values for charm counting  $n_c(B^0)$  seems slightly larger than the experimental data though it is still consistent within the errors. The resulting prediction for the CKM matrix element  $|V_{cb}|$  agrees well with the one extracted from the exclusive decays[12].

In summary, it has been shown that the endpoint behavior may be smoothed by a curve fitting method. Their contributions are in general small. The considerations and numerical predictions in the previous papers[3, 4] within the framework of HQEFT of QCD are justified to be reliable. Here the inclusion of the endpoint effects makes the prediction on the lifetime differences and the extraction on the CKM matrix element  $|V_{cb}|$  more precise.

### Acknowledgement

This work was supported in part by the key projects of Chinese Academy of Sciences, the National Science Foundation of China (NSFC).

## References

- [1] Y. L. Wu, Mod. Phys. Lett. **A 8** (1993) 819.
- [2] Y. L. Wu, Y. A. Yan, M. Zhong, Y. B. Zuo, W. Y. Wang, Mod. Phys. Lett. **A 18** (2003) 1303.
- [3] Y.A Yan, Y.L Wu and W.Y Wang, *Int.J.Mod.Phys.* **A15**: 2735-2770, 2000.
- [4] Y.L Wu and Y.A Yan, *Int.J.Mod.Phys.***A16**:285-302,2001.
- [5] C.H.Jin, W.F.Palmer and E.A.Paschos, Phys.Lett. **B329** (1994) 364-368
- [6] C.H.Jin, W.F.Palmer and E.A.Paschos, hep-ph/9406361
- [7] A.Manohar and M.Wise, *Phys.Rev.***D 49**(1994),1310.

- [8] M.Luke, M.Savage, and M.Wise, *Phys.Lett.* **B 343**(1995), 329; *Phys.Lett.* **B 345**(1995), 301.
- [9] M.Lu, M.Luke, M.Savage, and B.Smith, *Phys.Rev.* **D 55**(1997), 2827.
- [10] K.Hagiwara *et al*, *Phys.Rev.* **D 66**, 010001 (2002).
- [11] CLEO Collaboration ( T. E. Coan *et al.* ), *Phys.Rev.Lett.* **80**,1151 (1998).
- [12] W. Y. Wang, Y. L. Wu, Y. A. Yan, *Int. J. Mod. Phys.* **A 15** (2000) 1817;  
W.Y. Wang, Y.L. Wu, Y.A. Yan, M. Zhong, Y.B. Zuo; hep-ph/0310266.

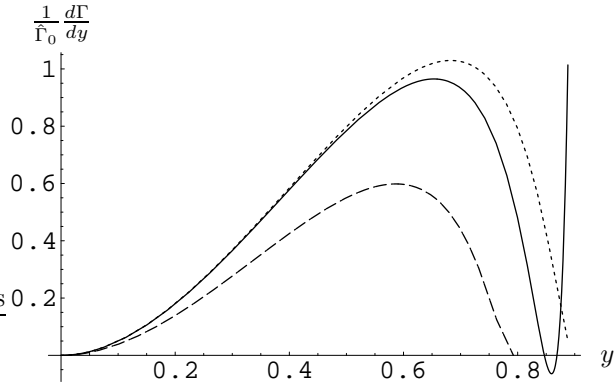


Figure 1: Comparison of lepton spectrums in HQEFT with the one in free quark model. The solid line and the dashed line are obtained using heavy quark expansion to the next leading order and to the leading order respectively, whereas the dash dot line shows the prediction of the free quark model.

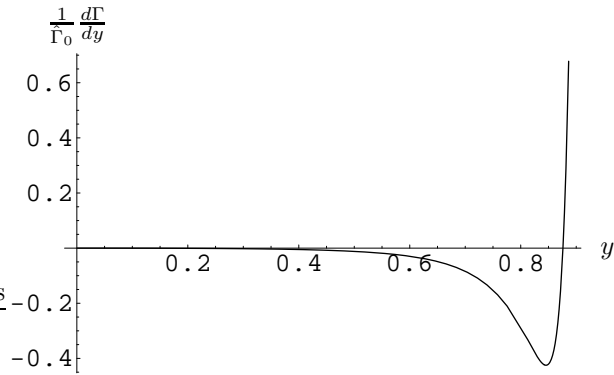


Figure 2: The correction of the next leading order to the leading order of heavy quark expansion in HQEFT.

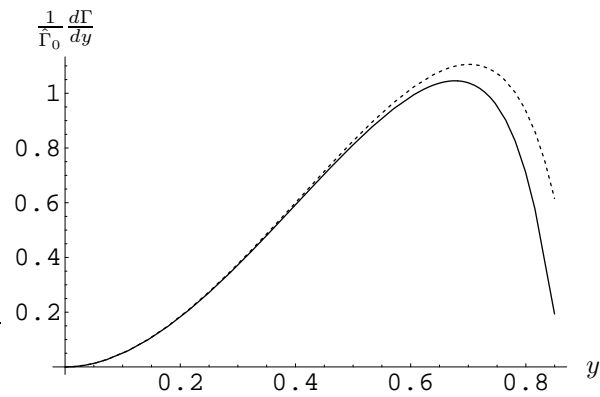


Figure 3: The lepton spectrums predicted by heavy quark expansion in HQEFT corresponding to  $\Lambda_b$  decay. The dashed line comes from the leading order in heavy quark expansion and the solid one includes the contribution from the next leading order.

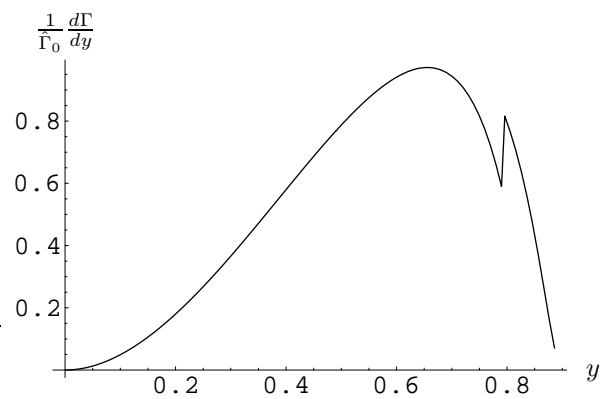


Figure 4: The lepton spectrum with the part in endpoint region replaced by the result of leading order.

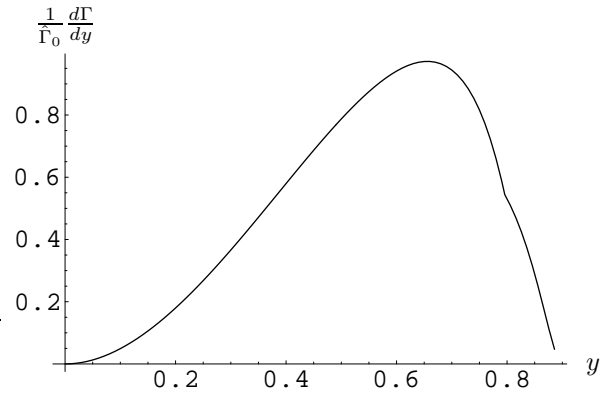


Figure 5: The lepton spectrum obtained after multiplying a rescaling factor.

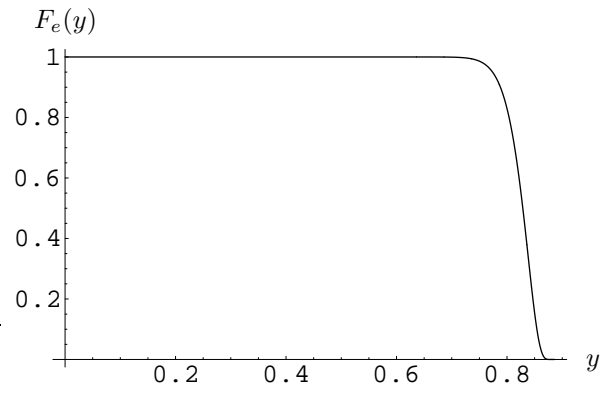


Figure 6: The function introduced to make lepton spectrum come to zero at the end point.

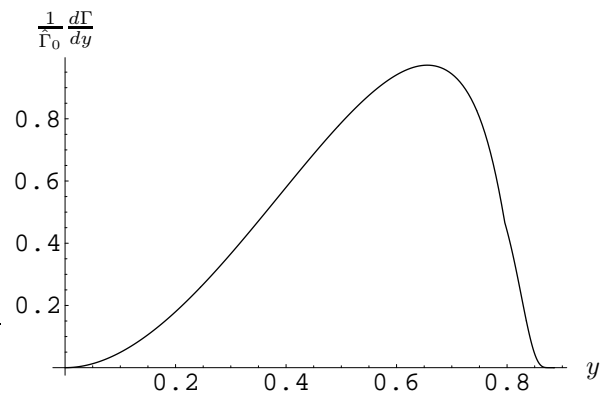


Figure 7: The lepton spectrum obtained in scheme 1.

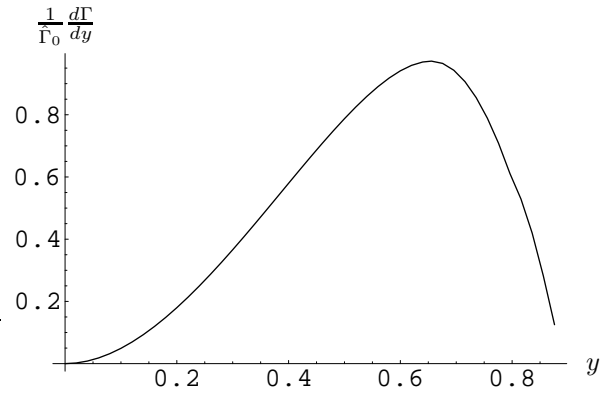


Figure 8: The counterpart of Figure 5 in scheme 2.

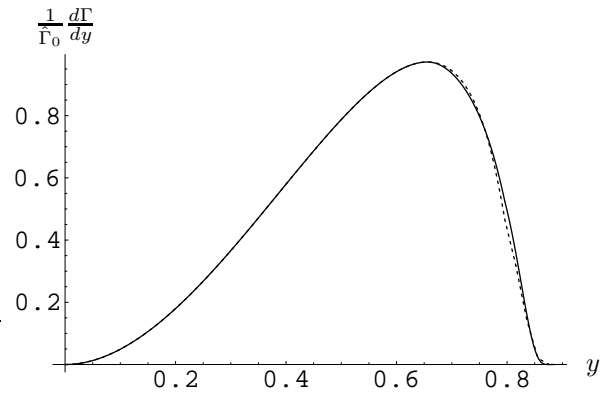


Figure 9: The lepton spectrum obtained in scheme 2, where the spectrum in scheme 1 is also given for comparison ( shown in the dashed line ) .

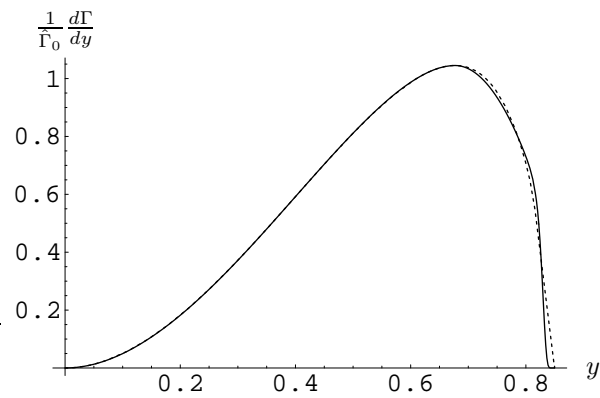


Figure 10: The same as Figure 9 but for  $\Lambda_b$  decays.

$m_c(Gev)$	1.55			1.65			1.75			1.8		
$\kappa_1(Gev^2)$	-0.55	-0.65	-0.75	-0.45	-0.55	-0.65	-0.4	-0.5	-0.6	-0.35	-0.45	-0.55
$\frac{\tau(\Lambda_b)}{\tau(B^0)}$	0.814	0.820	0.826	0.797	0.803	0.809	0.781	0.788	0.795	0.770	0.778	0.785
$B_{SL}(B^0)(\%)$	9.53	9.41	9.28	9.79	9.67	9.55	10.01	9.89	9.78	10.15	10.04	9.92
$B_\tau(B^0)$	0.026	0.025	0.024	0.026	0.025	0.023	0.025	0.024	0.023	0.025	0.023	0.022
$R(B^0)$	0.27	0.27	0.26	0.27	0.26	0.24	0.25	0.24	0.24	0.25	0.23	0.22
$n_c(B^0)$	1.24	1.25	1.26	1.22	1.23	1.24	1.20	1.21	1.22	1.19	1.20	1.21
$B_{SL}(\Lambda_b)(\%)$	10.25	10.17	10.09	10.45	10.37	10.30	10.61	10.55	10.49	10.72	10.66	10.60
$B_\tau(\Lambda_b)$	0.034	0.033	0.032	0.034	0.033	0.032	0.033	0.032	0.031	0.033	0.032	0.031
$R(\Lambda_b)$	0.33	0.32	0.32	0.33	0.32	0.31	0.31	0.30	0.30	0.31	0.30	0.29
$n_c(\Lambda_b)$	1.18	1.18	1.19	1.16	1.17	1.17	1.15	1.15	1.16	1.14	1.15	1.15
$\frac{B_{SL}(\Lambda_b)}{B_{SL}(B^0)}$	1.08	1.08	1.09	1.07	1.07	1.08	1.06	1.07	1.07	1.06	1.06	1.07
$ V_{cb} (10^{-2})$	3.94	4.02	4.11	4.02	4.11	4.20	4.15	4.25	4.34	4.20	4.30	4.40

Table 1: The observable quantities of  $B^0, \Lambda_b$  decay in scheme 1, where  $\mu = \frac{1}{2}m_b$ .

$m_c(Gev)$	1.55			1.65			1.75			1.8		
$\kappa_1(Gev^2)$	-0.55	-0.65	-0.75	-0.45	-0.55	-0.65	-0.4	-0.5	-0.6	-0.35	-0.45	-0.55
$\frac{\tau(\Lambda_b)}{\tau(B^0)}$	0.804	0.809	0.814	0.787	0.793	0.799	0.772	0.779	0.785	0.762	0.769	0.776
$B_{SL}(B^0)(\%)$	11.71	11.58	11.45	12.00	11.87	11.75	12.24	12.12	12.00	12.39	12.28	12.16
$B_\tau(B^0)$	0.031	0.030	0.029	0.031	0.030	0.028	0.030	0.029	0.027	0.030	0.028	0.027
$R(B^0)$	0.26	0.26	0.25	0.26	0.25	0.24	0.25	0.24	0.23	0.24	0.23	0.22
$n_c(B^0)$	1.21	1.22	1.23	1.19	1.20	1.21	1.18	1.19	1.20	1.17	1.18	1.19
$B_{SL}(\Lambda_b)(\%)$	12.46	12.38	12.30	12.68	12.60	12.53	12.85	12.80	12.73	12.97	12.91	12.85
$B_\tau(\Lambda_b)$	0.040	0.039	0.038	0.040	0.039	0.038	0.039	0.038	0.037	0.039	0.038	0.037
$R(\Lambda_b)$	0.32	0.32	0.31	0.32	0.31	0.30	0.30	0.30	0.29	0.30	0.29	0.29
$n_c(\Lambda_b)$	1.15	1.16	1.17	1.14	1.15	1.15	1.13	1.13	1.14	1.12	1.13	1.13
$\frac{B_{SL}(\Lambda_b)}{B_{SL}(B^0)}$	1.06	1.07	1.07	1.06	1.06	1.07	1.05	1.06	1.06	1.05	1.05	1.06
$ V_{cb} (10^{-2})$	3.70	3.78	3.86	3.78	3.86	3.94	3.90	3.99	4.08	3.95	4.04	4.13

Table 2: The observable quantities of  $B^0, \Lambda_b$  decay in scheme 1, where  $\mu = m_b$ .

$m_c(Gev)$	1.55			1.65			1.75			1.8		
$\kappa_1(Gev^2)$	-0.55	-0.65	-0.75	-0.45	-0.55	-0.65	-0.4	-0.5	-0.6	-0.35	-0.45	-0.55
$\mu(GeV)$	2.83	2.94	3.06	2.61	2.70	2.80	2.46	2.54	2.62	2.38	2.44	2.52
$\frac{\tau(\Lambda_b)}{\tau(B^0)}$	0.810	0.815	0.820	0.794	0.800	0.805	0.779	0.786	0.792	0.769	0.776	0.783
$B_\tau(B^0)$	0.028	0.027	0.026	0.027	0.026	0.025	0.026	0.025	0.024	0.025	0.024	0.023
$R(B^0)$	0.27	0.26	0.25	0.26	0.25	0.24	0.25	0.24	0.23	0.24	0.23	0.22
$n_c(B^0)$	1.23	1.24	1.24	1.21	1.22	1.23	1.20	1.21	1.21	1.19	1.20	1.20
$B_{SL}(\Lambda_b)(\%)$	11.23	11.27	11.32	11.15	11.20	11.25	11.08	11.15	11.20	11.06	11.10	11.17
$B_\tau(\Lambda_b)$	0.037	0.036	0.035	0.036	0.035	0.034	0.034	0.034	0.033	0.034	0.033	0.032
$R(\Lambda_b)$	0.33	0.32	0.31	0.32	0.31	0.30	0.31	0.30	0.29	0.31	0.30	0.29
$n_c(\Lambda_b)$	1.17	1.17	1.18	1.15	1.16	1.16	1.14	1.15	1.15	1.14	1.14	1.15
$\frac{B_{SL}(\Lambda_b)}{B_{SL}(B^0)}$	1.07	1.08	1.08	1.06	1.07	1.07	1.06	1.06	1.07	1.06	1.06	1.07
$ V_{cb} (10^{-2})$	3.83	3.89	3.96	3.94	4.01	4.08	4.09	4.17	4.25	4.16	4.24	4.32

Table 3: The observable quantities of  $B^0, \Lambda_b$  decay in scheme 1, where  $\mu$  have been chosen to satisfy  $B_{SL}(B^0) = 10.48\%$ .

$m_c(Gev)$	1.55			1.65			1.75			1.8		
$\kappa_1(Gev^2)$	-0.55	-0.65	-0.75	-0.45	-0.55	-0.65	-0.4	-0.5	-0.6	-0.35	-0.45	-0.55
$\frac{\tau(\Lambda_b)}{\tau(B^0)}$	0.811	0.816	0.822	0.793	0.800	0.806	0.778	0.785	0.792	0.767	0.775	0.782
$B_{SL}(B^0)(\%)$	10.32	10.20	10.07	10.60	10.48	10.35	10.83	10.71	10.59	10.97	10.86	10.74
$B_\tau(B^0)$	0.028	0.027	0.026	0.028	0.026	0.025	0.027	0.025	0.024	0.026	0.025	0.024
$R(B^0)$	0.27	0.26	0.26	0.26	0.25	0.24	0.25	0.23	0.23	0.24	0.23	0.22
$n_c(B^0)$	1.23	1.24	1.25	1.21	1.22	1.23	1.19	1.20	1.21	1.18	1.19	1.20
$B_{SL}(\Lambda_b)(\%)$	11.06	10.98	10.90	11.28	11.20	11.12	11.44	11.38	11.31	11.55	11.49	11.43
$B_\tau(\Lambda_b)$	0.036	0.035	0.034	0.036	0.035	0.034	0.035	0.034	0.033	0.035	0.034	0.033
$R(\Lambda_b)$	0.33	0.32	0.31	0.32	0.31	0.31	0.31	0.30	0.29	0.30	0.30	0.29
$n_c(\Lambda_b)$	1.17	1.17	1.18	1.15	1.16	1.17	1.14	1.15	1.15	1.13	1.14	1.14
$\frac{B_{SL}(\Lambda_b)}{B_{SL}(B^0)}$	1.07	1.08	1.08	1.06	1.07	1.07	1.06	1.06	1.07	1.05	1.06	1.06
$ V_{cb} (10^{-2})$	3.85	3.93	4.01	3.92	4.01	4.10	4.05	4.15	4.24	4.10	4.19	4.29

Table 4: The observable quantities of  $B^0, \Lambda_b$  decay in scheme 1, where  $\mu = 2.70Gev$ .

$m_c(Gev)$	1.55			1.65			1.75			1.8		
$\kappa_1(Gev^2)$	-0.55	-0.65	-0.75	-0.45	-0.55	-0.65	-0.4	-0.5	-0.6	-0.35	-0.45	-0.55
$\frac{\tau(\Lambda_b)}{\tau(B^0)}$	0.820	0.827	0.833	0.802	0.809	0.816	0.786	0.794	0.802	0.775	0.784	0.792
$B_{SL}(B^0)(\%)$	9.51	9.39	9.26	9.77	9.65	9.53	9.99	9.87	9.75	10.13	10.02	9.90
$B_\tau(B^0)$	0.026	0.025	0.024	0.026	0.025	0.024	0.025	0.024	0.023	0.025	0.024	0.023
$R(B^0)$	0.27	0.27	0.26	0.27	0.26	0.25	0.25	0.24	0.24	0.25	0.24	0.23
$n_c(B^0)$	1.24	1.25	1.26	1.22	1.23	1.24	1.20	1.21	1.22	1.19	1.20	1.21
$B_{SL}(\Lambda_b)(\%)$	10.24	10.15	10.07	10.44	10.36	10.29	10.59	10.54	10.47	10.70	10.64	10.58
$B_\tau(\Lambda_b)$	0.034	0.033	0.032	0.034	0.033	0.032	0.033	0.032	0.031	0.033	0.032	0.031
$R(\Lambda_b)$	0.33	0.33	0.32	0.33	0.32	0.31	0.31	0.30	0.30	0.31	0.30	0.29
$n_c(\Lambda_b)$	1.18	1.18	1.19	1.16	1.17	1.17	1.15	1.15	1.16	1.14	1.15	1.15
$\frac{B_{SL}(\Lambda_b)}{B_{SL}(B^0)}$	1.08	1.08	1.09	1.07	1.07	1.08	1.06	1.07	1.07	1.06	1.06	1.07
$ V_{cb} (10^{-2})$	3.93	4.01	4.09	4.02	4.10	4.18	4.15	4.24	4.33	4.20	4.29	4.39

Table 5: The observable quantities of  $B^0, \Lambda_b$  decay in scheme 2, where  $\mu = \frac{1}{2}m_b$ .

$m_c(Gev)$	1.55			1.65			1.75			1.8		
$\kappa_1(Gev^2)$	-0.55	-0.65	-0.75	-0.45	-0.55	-0.65	-0.4	-0.5	-0.6	-0.35	-0.45	-0.55
$\frac{\tau(\Lambda_b)}{\tau(B^0)}$	0.810	0.816	0.822	0.793	0.799	0.806	0.777	0.784	0.791	0.767	0.775	0.782
$B_{SL}(B^0)(\%)$	11.69	11.56	11.42	11.98	11.85	11.72	12.21	12.10	11.97	12.37	12.25	12.13
$B_\tau(B^0)$	0.032	0.030	0.029	0.031	0.030	0.029	0.030	0.029	0.027	0.030	0.028	0.027
$R(B^0)$	0.27	0.26	0.25	0.26	0.25	0.25	0.25	0.24	0.23	0.24	0.23	0.22
$n_c(B^0)$	1.21	1.22	1.23	1.19	1.20	1.21	1.18	1.19	1.20	1.17	1.18	1.19
$B_{SL}(\Lambda_b)(\%)$	12.45	12.36	12.28	12.67	12.59	12.51	12.83	12.78	12.71	12.95	12.89	12.83
$B_\tau(\Lambda_b)$	0.041	0.040	0.038	0.040	0.039	0.038	0.039	0.038	0.037	0.039	0.038	0.037
$R(\Lambda_b)$	0.33	0.32	0.31	0.32	0.31	0.30	0.30	0.30	0.29	0.30	0.29	0.29
$n_c(\Lambda_b)$	1.15	1.16	1.17	1.14	1.15	1.15	1.13	1.13	1.14	1.12	1.13	1.13
$\frac{B_{SL}(\Lambda_b)}{B_{SL}(B^0)}$	1.07	1.07	1.08	1.06	1.06	1.07	1.05	1.06	1.06	1.05	1.05	1.06
$ V_{cb} (10^{-2})$	3.70	3.77	3.84	3.77	3.85	3.93	3.90	3.98	4.07	3.95	4.03	4.12

Table 6: The observable quantities of  $B^0, \Lambda_b$  decay in scheme 2, where  $\mu = m_b$ .

$m_c(Gev)$	1.55			1.65			1.75			1.8		
$\kappa_1(Gev^2)$	-0.55	-0.65	-0.75	-0.45	-0.55	-0.65	-0.4	-0.5	-0.6	-0.35	-0.45	-0.55
$\mu(GeV)$	2.84	2.96	3.08	2.63	2.72	2.82	2.48	2.55	2.64	2.39	2.46	2.53
$\frac{\tau(\Lambda_b)}{\tau(B^0)}$	0.816	0.821	0.827	0.799	0.806	0.812	0.784	0.792	0.798	0.774	0.782	0.789
$B_\tau(B^0)$	0.028	0.028	0.027	0.028	0.027	0.026	0.026	0.025	0.024	0.026	0.025	0.024
$R(B^0)$	0.27	0.27	0.26	0.27	0.26	0.25	0.25	0.24	0.23	0.25	0.24	0.23
$n_c(B^0)$	1.23	1.24	1.25	1.21	1.22	1.23	1.20	1.21	1.22	1.19	1.20	1.21
$B_{SL}(\Lambda_b)(\%)$	11.23	11.28	11.33	11.17	11.21	11.26	11.10	11.15	11.21	11.06	11.12	11.16
$B_\tau(\Lambda_b)$	0.037	0.036	0.036	0.036	0.035	0.035	0.034	0.034	0.033	0.034	0.033	0.032
$R(\Lambda_b)$	0.33	0.32	0.32	0.32	0.31	0.31	0.31	0.30	0.29	0.31	0.30	0.29
$n_c(\Lambda_b)$	1.17	1.17	1.18	1.15	1.16	1.17	1.15	1.15	1.15	1.14	1.14	1.15
$\frac{B_{SL}(\Lambda_b)}{B_{SL}(B^0)}$	1.07	1.08	1.08	1.07	1.07	1.07	1.06	1.06	1.07	1.06	1.06	1.06
$ V_{cb} (10^{-2})$	3.82	3.88	3.94	3.93	4.00	4.07	4.09	4.16	4.24	4.15	4.23	4.31

Table 7: The observable quantities of  $B^0, \Lambda_b$  decay in scheme 2, where  $\mu$  have been chosen to satisfy  $B_{SL}(B^0) = 10.48\%$ .

$m_c(Gev)$	1.55			1.65			1.75			1.8		
$\kappa_1(Gev^2)$	-0.55	-0.65	-0.75	-0.45	-0.55	-0.65	-0.4	-0.5	-0.6	-0.35	-0.45	-0.55
$\frac{\tau(\Lambda_b)}{\tau(B^0)}$	0.817	0.823	0.829	0.799	0.806	0.813	0.783	0.791	0.798	0.772	0.780	0.788
$B_{SL}(B^0)(\%)$	10.33	10.20	10.07	10.60	10.48	10.36	10.83	10.71	10.59	10.98	10.86	10.74
$B_\tau(B^0)$	0.028	0.027	0.026	0.028	0.027	0.025	0.027	0.026	0.024	0.027	0.025	0.024
$R(B^0)$	0.27	0.26	0.26	0.26	0.26	0.24	0.25	0.24	0.23	0.25	0.23	0.22
$n_c(B^0)$	1.23	1.24	1.25	1.21	1.22	1.23	1.19	1.20	1.21	1.18	1.19	1.20
$B_{SL}(\Lambda_b)(\%)$	11.08	10.99	10.91	11.29	11.21	11.13	11.45	11.39	11.32	11.56	11.50	11.44
$B_\tau(\Lambda_b)$	0.036	0.035	0.034	0.036	0.035	0.034	0.035	0.034	0.033	0.035	0.034	0.033
$R(\Lambda_b)$	0.32	0.32	0.31	0.32	0.31	0.31	0.31	0.30	0.29	0.30	0.30	0.29
$n_c(\Lambda_b)$	1.17	1.18	1.18	1.15	1.16	1.17	1.14	1.15	1.15	1.13	1.14	1.15
$\frac{B_{SL}(\Lambda_b)}{B_{SL}(B^0)}$	1.07	1.08	1.08	1.07	1.07	1.07	1.06	1.06	1.07	1.05	1.06	1.07
$ V_{cb} (10^{-2})$	3.84	3.91	3.99	3.92	4.00	4.08	4.05	4.13	4.22	4.10	4.19	4.28

Table 8: The observable quantities of  $B^0, \Lambda_b$  decay in scheme 2, where  $\mu = 2.72Gev$ .